Journal of the Brazilian Society of Mechanical Sciences and Engineering (2021) 43:297
https://doi.org/10.1007/s40430-021-03007-3

ANALYSIS OF VORTEX CORE GENERATION IN PIPE FLOWS UNDER DIFFERENT REYNOLDS NUMBER CONDITIONS

Salvador, F.J., Carreres, M., Quintero, P., González-Montero, L.A. (*)

CMT-Motores Térmicos, Universitat Politècnica de València

Camino de Vera s/n, E-46022 Spain

(*) Corresponding author:

Lucas González, lugonmon@mot.upv.es

CMT-Motores Térmicos, Universitat Politècnica de València

Camino de Vera s/n, E-46022 Spain

ABSTRACT

Pipe flow is a well-documented case widely studied in both theoretical and practical applications. The present work aims at studying the influence of the Reynolds number on turbulent vortex distribution using Large Eddy Simulations (LES). Features such as the mean velocity profiles and root-mean squared velocity are first numerically investigated for different fluid properties involving Reynolds numbers ranging from 5,925 to 15,190 in order to verify the law-of-the-wall and turbulence statistics with experimental and DNS data. Once the simulations are validated, the vortex core generation within the flow is studied through a detection algorithm based on the λ_2 criterion with two different approaches, first using an absolute threshold value and then using a relative threshold value depending on the turbulent intensity. Results are compared in terms of number of structures and Probability Density Functions for both the size and the radial distributions. Finally, results are compared for one condition with the Q-criterion to assess the results obtained resulting in practically identical volume and radial distributions. These results are deemed to shed light on the vortex formation and location to generate proper inflow boundary conditions to highly resolved simulations in varied engineering applications.

KEYWORDS

Computational, LES, pipe flow, turbulence, vortex detection

DECLARATIONS

Funding: This research has been funded by the Spanish Ministerio de Economía y Competitividad through the project RTI2018-099706-B-100: “Estudio de la atomización primaria mediante simulaciones DNS y técnicas ópticas de muy alta resolución” and the Spanish Ministerio de Ciencia e innovación through the project EQC2018-004605-P: “Estudio del proceso de inyección en atmosferas presurizadas”. The authors thankfully acknowledge the computer resources from the Rigel cluster at UPV (Spain) and the Bebop cluster from the Laboratory Computing Resource Center at Argonne National Laboratory (USA).

Competing interests: the authors declare that they have no known competing financial interests or personal relationships that could have appeared to influence the work reported in this paper.

Availability of data and material: data will be made available on request.

Code availability: The code used is OpenFOAM v3.0.0.

LIST OF NOTATIONS

u_τ	friction velocity
R	pipe radius
Re_τ	Kármán number
Re_D	Reynolds number
L	pipe length
D	pipe diameter
$\bar{u}_i$	resolved velocity vector
$\bar{p}$	modified kinetic pressure
C_w	WALE constant
$\bar{S}_{ij}$	resolved strain rate tensor
S	symmetric strain rate tensor
U_b	bulk velocity
y^+	non-dimensional distance to the wall
r_{wall}^+	cell size in radial direction on the wall in wall units

x^+ cell size in axial direction in wall units

r radial position

u_x axial velocity

$u_{x,cl}$ axial velocity on the centerline

u_x^+ axial velocity in wall units

$u_{x,rms}^+$ axial root mean squared velocity in wall units

f friction factor

N_s number of structures

GREEK SYMBOLS

τ_w wall shear stress

ρ density

ν kinematic viscosity

ν_t turbulent viscosity

Δ width of the LES filter

Ω antisymmetric rate-of-rotation tensor

μ dynamic viscosity

ω_{wall}^+ cell size in azimuthal direction on the wall in wall units

ξ non-dimensional radial position

ξ^+ non-dimensional radial position in wall units

ABBREVIATIONS

DNS Direct Numerical Simulations

ECN Engine Combustion Network

SGS SubGrid Scale

WALE Wall Adapting Local Eddy-viscosity

LES Large Eddy Simulations

CFL Courant-Friedrich-Lewis

PDF Probability Density Function

1. INTRODUCTION

Most turbulent flows in engineering applications are wall-bounded, at least partially. Over the years, the interaction between viscous turbulent flows and solids has been studied in several problems. Regarding wall-bounded flows, there are three canonical flows that represent the purest interaction between these two worlds: the spatially evolving boundary layer, the channel flow, and the pipe flow.

The importance of the presence of a solid within the flow is that the behaviour of the mean velocity profile is affected: near the wall, viscous effects are important and the scaling factor depends on the friction velocity $u_\tau = \sqrt{\tau_w/\rho}$ and the wall length scale ν/u_τ, where τ_w is the wall shear stress whereas ρ and ν are the fluid density and kinematic viscosity, respectively. In the outer region, the appropriate length scale is the pipe radius (R), whereas the velocity scale remains being u_τ since it is the inner boundary condition for the outer flow [1, 2]. Therefore, a specific Reynolds number based on those parameters and known as the Kármán number may be defined and particularized for pipe flows as $Re_\tau = u_\tau R/\nu$. Traditionally, the study of the turbulence in these flows has been carried out by means of experimental works, as done by Eggels [3] and den Toonder [4] back in mid 90s. More recently, there have been experimental works about high Reynolds pipe flows in the so-called "Superpipe" located at Princeton [5][6] or the CICLoPE project [7] where Örlü et al. [8] performed How-wire measurements and conclude that their results supported the attached-eddy hypothesis for the scaling of the Reynolds stress tensor. But the increasing capabilities in terms of computational processing power are also driving advances in the theoretical approach of the inner flow turbulence study from a numerical standpoint. First Direct Numerical Simulations were performed by Eggels et al. [3] who compared DNS results against their own experimental data for a bulk based Reynolds number (Re_D) of 5,300. Even though their results matched their experimental data, they also compared them with the work of Kim et al. [9], who worked with the same conditions on turbulent channel flow. The following studies of this kind of flows analyzed two different parameters that control the turbulence spectra. On the one hand, the pipe length (L) to pipe radius (R) ratio; on the other hand, the Reynolds number. Several studies [10–12] investigated the influence of the domain on capturing all the turbulent structures. These studies used pipe lengths ranging from $5R$ to $30R$. Kim et al. [10] found that a length of 7.5 L/D should be enough to capture all the turbulent processes in pipe flows. Additionally, there are several studies about the influence of the Reynolds number on the turbulent statistics. For instance, El Khoury et al. [13] performed DNS simulations from low to moderate Reynolds numbers and compared them with other results of DNS on pipe flows [14, 15] and with the other two canonical wall-bounded flows [16, 17].

Even though there exist many works on this canonical flow, there are still many insights that remain unclarified. For instance, the characteristic peak of the root-mean-squared of the streamwise velocity fluctuations seems to be nearly constant with the Reynolds number, but there is no conclusive evidence to support it, as reviewed by some authors [2, 18].

These uncertainties bring up new different approaches to the study of turbulence in this kind of flows. Hellström et al. [19] applied Proper Orthogonal Decomposition (POD) to experimental data in order to study the self-similarity behaviour of the radial POD resulting in a single length scale representing the complete structure. A similar approach was conducted by Abreu et al. [20], who applied Spectral POD and resolvent analysis to DNS results from El Khoury et al. [13] to study the characteristic elongated structures corresponding to near-wall streamwise vortices and streaks. Also, some studies have been performed on structure detection, as the one performed by Hwang et al. [21] where they demonstrate the logarithmic region by statistically studying the coherent structures attached to the wall.

LES and DNS have proven their key role on the study of turbulent flows for fundamental and engineering applications. Their versatility allows studying theoretical situations that simplify the problems and help isolating the effects that in reality use to take place combined with other processes (e.g. using flat velocity profiles to purely study solid or liquid interactions). However, in most real applications the different processes that take place in one problem feedback with each other and lead to a very different behaviour that cannot be predicted on the isolated study.

Over the last years, different techniques have been used to feed the LES and DNS simulations with coherent velocity fields capable to correctly trigger the turbulence within the domain as reviewed by Dhamankar et al. [22]. From their work, two approaches can be highlighted: the use of synthetic boundary conditions through digital filters, as proposed by Klein et al. [23]; or mapping a turbulent database from a prior computation or experiment. Both approaches have been applied to wide range of problems. For instance, synthetic boundary conditions were used on [24, 25] to study primary breakup and particle laden respectively, and mapped boundary conditions were used in [26, 27] . In particular, Payri et al. [26] studied the atomization process of the ECN Spray A [28] through DNS using both methods. When comparing them, they noticed that the injected turbulent structures showed a very different shape, importantly influencing droplet generation. While the synthetic vortex had annular shape, the turbulence mapped from a previous pipe flow LES showed axially elongated structures.

In this framework, considering that using fair synthetic turbulent statistics does not ensure the proper shape of the generated structures, the main objective of this paper is to investigate the influence of the Reynolds conditions on the vortex structures formation through widely known tools. Also, since DNS are currently limited to low to moderate Reynolds numbers, a parametric study has been carried out for the 5,925 to 15,190 range. These results can be used to compare the structures generated by a pipe flow synthetic boundary condition when using them or when generating new synthetic turbulence models for these cases.

The paper is structured as follows. **Section 2** is a description of the numerical method and sub-grid model used to carry out the simulations. In **Section 3**, the computational and physical parameters are presented for all the simulations, including the spatial domain and the computational grid parameters. **Section 4** discusses the results through two main approaches. First, a validation of the results by comparing them with the law of the wall theory and the friction factor is done. Once the data are validated, a deeper study on the turbulence side intends to shed light on the vortex size and radial distribution. Finally, **Section 5** wraps up the conclusions and points out the directions for future studies.

2. NUMERICAL METHODS

As stated in Section 3, the study focuses on isothermal and incompressible flow conditions. Considering a Newtonian fluid, the governing equations of the problem are then the continuity (1) and the momentum (2) equations:

$$\frac{\partial}{\partial x_i}(\bar{u}_i) = 0 \tag{1}$$

$$\frac{\partial \bar{u}_i}{\partial t} + \frac{\partial}{\partial x_j}\left(\bar{u}_i\,\bar{u}_j\right) = -\frac{1}{\rho}\frac{\partial \bar{p}}{\partial x_j} + \frac{\partial}{\partial x_j}\left((\nu+\nu_t)\left(\frac{\partial \bar{u}_i}{\partial x_j} + \frac{\partial \bar{u}_j}{\partial x_i}\right)\right) \tag{2}$$

Where $\bar{u}_i$ is the resolved velocity field and $\bar{p}$ is the modified kinetic pressure. The closure of Eq. (2) is given by the Subgrid Scale (SGS) viscosity (ν_t), which is a non-linear term that needs to be modelled. There are many subgrid models to estimate the energy dissipation in the subgrid range. Given the conditions of the problem and the objective of the study, the Wall Adapting Local Eddy-viscosity (WALE) model [29] is chosen. This model is based on the square of the velocity gradient tensor to estimate the local eddy viscosity through Eq. (3) and is deemed to properly handle the transition from laminar to turbulent flow:

$$\nu_t = (C_w \Delta)^2 \frac{\left(\bar{S}_{ij}^d \bar{S}_{ij}^d\right)^{3/2}}{\left(\bar{S}_{ij}\,\bar{S}_{ij}\right)^{5/2} + \left(\bar{S}_{ij}^d\,\bar{S}_{ij}^d\right)^{5/4}} \tag{3}$$

where C_w is the WALE model constant (which allows calibrating the dissipation), Δ is the width of the LES filter and the last term depends on the traceless symmetric part of the squared gradient tensor $\bar{S}_{ij}^d$ and the resolved strain rate tensor $\bar{S}_{ij}$. About this last term, it is important to point out that it behaves as a cubic function of the wall-distance (y^3) and it is function of both the rotation and the strain rates. Hence, this model is capable of reproducing the near-wall scaling without any dynamic procedure and has proved its suitability to reproduce the turbulent flow behaviour in pipes [29] . The constant C_w is set to 0.5 as proposed by Nicoud and Ducros [29] for this flow topology.

All the simulations present in the document are performed using the standard PISO (Pressure Implicit with Splitting Operator) solver proposed by Issa [30] from the open source C++ library OpenFOAM 3.0.0 [31]. Second-order centred accurate discretization schemes are employed to compute gradients and Laplacian terms, whereas a second-order implicit scheme is used for time-stepping. A constant time step is used, set to $4 \cdot 10^{-9}$ s to ensure a CFL-number lower than 0.4 in the whole domain during the simulation time.

Concerning the study of the vortex structures generated within the fluid submitted to pipe flow, there exist several methods to detect local vortex, most of them being based on the analysis of the velocity gradient tensor $\nabla \boldsymbol{u}$. Among these methods, the λ_2 criterion proposed by Jeong and Hussain [32] has been chosen to discriminate the coherent structures for all conditions. Additionally, the Q-criterion has been applied to one of the test conditions in order to compare both criteria. λ_2 method starts by decomposing $\nabla \boldsymbol{u}$ into a symmetric rate-of-strain tensor (S) and an antisymmetric rate-of-rotation tensor (Ω). Neglecting the viscous effects and the unsteady irrotational straining, the symmetric part of the gradient of the incompressible Navier-Stokes equation can be expressed as established by Eq. (4).

$$S^2 + \Omega^2 = -\frac{1}{\rho}\nabla^2 p \tag{4}$$

Therefore, $S^2 + \Omega^2$ is a real and symmetric matrix and implies the existence of a local minimum of pressure. Due to its characteristics, the matrix has 3 eigenvalues ($\lambda_1 \geq \lambda_2 \geq \lambda_3$). It is established that a vortex core is a connected zone with two negative eigenvalues [32]. Since the eigenvalues are sorted in the decreasing order, this is equivalent to saying that a connected zone with $\lambda_2 < 0$ can be regarded to as a vortex structure.

On the other hand, the Q-criterion [33] defines an eddy as a region with a positive second invariant (Q) of $\nabla \boldsymbol{u}$. This term can be expressed as given by Eq. (5):

$$Q \equiv \frac{1}{2}(\|\Omega\|^2 - \|S\|^2) \tag{5}$$

which means that Q is a balance between shear strain rate and vorticity magnitude, becoming 0 at the wall.

3. SIMULATION PARAMETERS

3.1 Domain

In order to study a fully developed turbulent pipe flow, calculations are performed over a straight pipe under isothermal and incompressible flow conditions. The computational domain consists of a pipe of constant circular cross-section with radius R and length $16R$. Its coordinates are defined as *x* in the streamwise direction and *y* and *z* in the lateral directions, as shown in Figure 1a).

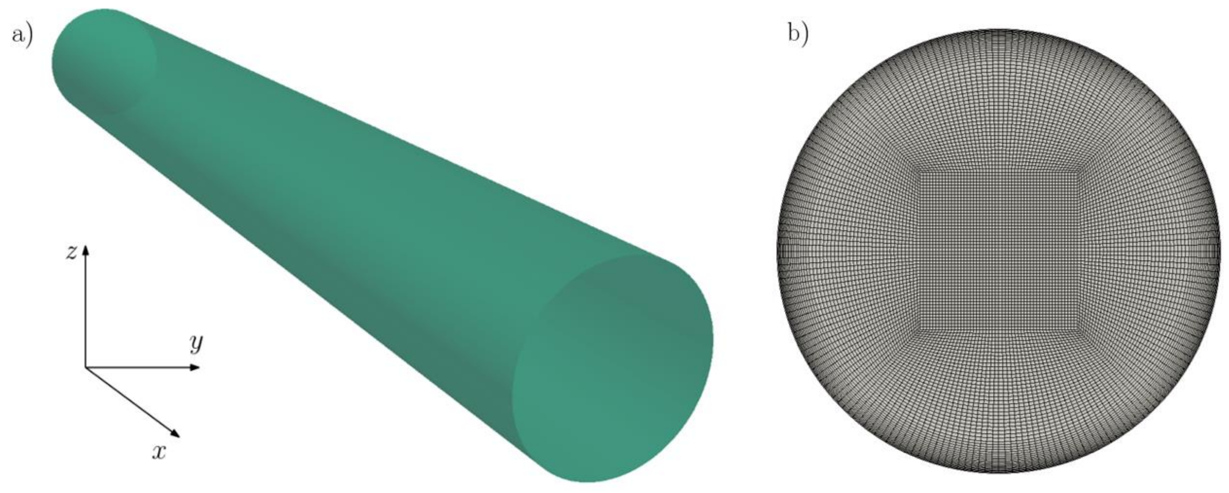

Figure 1: Computational domain and mesh scheme.

3.2. Boundary conditions

With the objective of reaching a fully developed turbulent flow within the computational domain, a cyclic boundary condition is used both at the inlet and the outlet. This way, the values at the outflow section are used as input conditions at the inflow section. Once the simulation completes around 1,000 washouts (a wash-out time being the interval that a particle remains in the computational domain before passing through the outflow section), the mean velocity profile is checked to match the typical developed turbulent pipe flow profile. Finally, a wall boundary condition is used in the cylindrical surface.

3.3. Initial conditions

In order to generate turbulence within the flow, a channel whose length matches the pipe length and whose side and height are equal to the pipe diameter is used. Turbulence is triggered in this preliminary domain using the boxTurb tool from OpenFOAM [31]. Once the turbulence is achieved in the channel, the result is mapped into the pipe domain. It is worth mentioning that, in order to achieve the final coherent turbulent flow in the pipe, it is necessary to simulate for around 200 washouts until the turbulent flow is fully adapted to the pipe domain. Once the turbulence is adapted to the new domain, the initial condition has been reached and the simulation can be started.

Name	$\boldsymbol{\rho\ [kg/m^3]}$	$\boldsymbol{\mu\ [kg/m \cdot s]}$	$\boldsymbol{\nu\ [m^2/s]}$	$\boldsymbol{Re_D}$
Ethanol	790	$1.2 \cdot 10^{-3}$	$1.52 \cdot 10^{-6}$	5,925
Pseudo-fluid	690	$0.69 \cdot 10^{-3}$	$1 \cdot 10^{-6}$	9,000
Isooctane	690	$0.5 \cdot 10^{-3}$	$7.25 \cdot 10^{-7}$	12,420
Heptane	686	$0.41 \cdot 10^{-3}$	$5.92 \cdot 10^{-7}$	15,190

Table 1. Fluid properties for each case of study.

3.4. Cases of study

Once the computational domain and boundary conditions are defined, it is important to set the physical conditions that concern the turbulence behaviour. The most widely non-dimensional number used to define the flow features is the Reynolds number. In order to vary its values from 5,925 to 15,190, the fluid properties have been modified keeping a constant bulk velocity $U_b = 100$ m/s. The fluid properties are listed in Table 1 (please note that a pseudo-fluid with properties deemed to improve and narrow down the comparison with the literature has been included).

3.5. Computational mesh

Figure 1b) also depicts the o-grid meshing strategy used to set up the numerical grid. When it comes to wall-bounded flows, a higher resolution is required in the normal direction of the boundary layer than in other parts on the domain. Even though the same strategy has been used for all the simulations, the cell sizes are different in each case: they have been set according to the first y^+, which in turn directly depends on the Reynolds number. Table 2 summarizes the parameters of the grid, being Δr^+_{wall}, $\Delta\omega^+_{wall}$ and Δx^+ the sizes (in wall units) of the wall cells in the normal, azimuthal and streamwise direction respectively. It is important to note that the non-dimensional magnitudes are based on the work by Nicoud and Ducros [29], which were used as a first mesh set up and were then calibrated with different cell grow factors and refinement in order to get the final mesh configuration. The mesh study was assessed for $Re_D = 5{,}925$ through the law-of-the-wall, as shown in Figure 2.

$\boldsymbol{Re_D}$	5,925	9,000	12,420	15,190
$\boldsymbol{N_{cells}}$	1,650,000	2,250,000	3,729,600	4,669,000
$\boldsymbol{\Delta r^+_{wall}}$	0.86	0.9	0.95	0.91
$\boldsymbol{\Delta\omega^+_{wall}}$	9.5	9	8.1	9.76
$\boldsymbol{\Delta x^+}$	24	24	24	24

Table 2. Mesh parameters for each case of study.

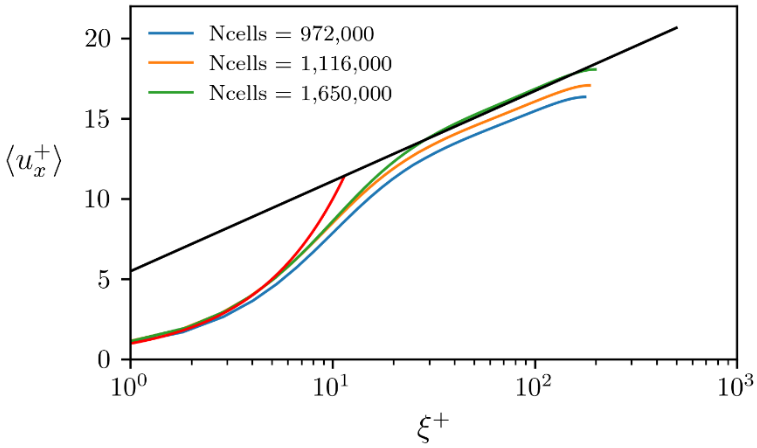

Figure 2: Mesh study for $Re_D = 5{,}925$

3.6 Mesh index of quality

In order to assess the quality of the LES resolution, an index of quality has been computed once each simulation was completed. There are three parameters on which the quality index can be based: kinetic energy, length scales and viscosity. In this work, the criterion based on the ratio between the kinetic energy resolved and the total kinetic energy is applied to assess the quality of the simulations. A LES is considered to possess good quality when at least the 80% [34] of the kinetic energy is resolved by the grid resolution ($IQ_k > 0.8$). The index of quality IQ_k is expressed at Eq. (6):

$$IQ_k = \frac{k_{res}}{k_{tot}} = \frac{k_{res}}{k_{res} + k_t + k_{num}} \tag{6}$$

where k_{res} is the kinetic energy resolved, k_t is the turbulent kinetic energy modelled by the subgrid model and k_{num} is the kinetic energy linked to the numeric error. The kinetic energy resolved can be easily computed with Eq. (7); the modelled part is evaluated with Eq. (8) proposed by Sagaut [35]; and the numerical part is estimated as suggested by Celik et al. [36] on a single grid according to Eq. (9).

$$k_{res} = \frac{1}{2}\left(u_{x,rms}^2 + u_{y,rms}^2 + u_{z,rms}^2\right) \tag{7}$$

$$k_t = \frac{1}{(C_m \Delta)^2} \nu_t \tag{8}$$

$$k_{num} \approx k_t \tag{9}$$

where C_m is a model constant whose value is set to 0.091. As shown in Eq. (7), temporal statistics need to be computed in order to obtain IQ_k. At this point, it is worth mentioning that all the mean parameters included in this document correspond to a plane located at half the pipe length, being temporally and azimuthally averaged in order to condense all the data in a single curve for each case.

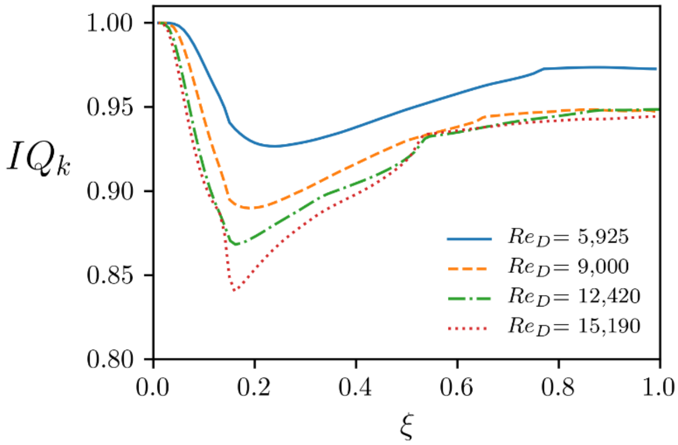

Figure 3: Index of Quality based on the turbulence resolution (IQ_k) for all tested cases.

Figure 3 depicts the evolution of IQ_k through the radial position defined as $\xi = (R - r)/R$. Please note that ξ is equal to 0 at the wall, being 1 at the centre of the pipe. It may be seen that all simulations have an IQ_k higher than 0.8 regardless of the radial location, implying a good quality of the calculations in each tested case. All computed cases present the minimum values located at the same point, where the grid topology changes. This means that the subgrid model models more energy in that region, whereas it has a lower influence on the results in the pipe centre and close to the wall. The LES quality has then been assessed based on the resolved kinetic energy in what constitutes the first validation of the calculations performed.

4. RESULTS AND DISCUSSION

4.1. Validation for fully developed turbulent pipe flow

One of the main objectives of this study is the analysis of the turbulent structures within the pipe flow. However, before visualizing the vortex distribution, it is important to fully validate the results obtained from the simulations. To this end, several parameters based on the mean velocity statistics are assessed in the present Section.

First, it is important to check that the mean velocity profile is developed, meaning that the simulation has reached a steady state. Figure 4a) shows the mean velocity profile in the streamwise direction normalized by the centreline velocity against the radial position ξ. It can be noticed that the profiles collapse at the centre of the pipe, the discrepancies being mainly found near the wall. This behaviour is well-known as addressed in the literature [37]. To ensure that the flow has been developed in the azimuthal direction, Figure 4b) displays the radial distribution of the standard deviation of the axial component of the velocity along this direction. Major deviations are found close to the wall regardless the case studied. Anyway, the values observed are very low for all cases, implying that the mean profiles are practically identical along the azimuthal direction and confirming the turbulence has reached a steady state.

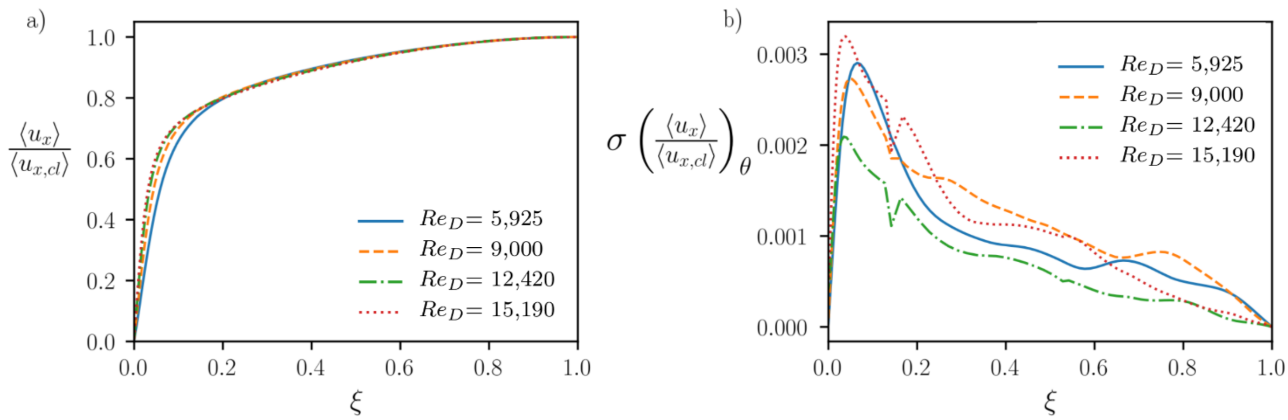

Figure 4: a) Mean axial velocity profile over the pipe radius for all tested conditions, b) standard deviation of the mean axial velocity profile in the azimuthal direction.

Once the steady state is reached, it is important to compute the friction parameters in order to further assess the reliability of the obtained results. Table 3 shows the results concerning the friction velocity and the Kármán number (Re_τ). The ratio between the friction velocity and the bulk velocity decreases as Re increases, in agreement with the results presented at [13]. This trend will also be seen when computing the friction factor.

Re_D	u_τ/U_b	Re_τ
5,925	0.671	199
9,000	0.635	286
12,420	0.607	377
15,190	0.592	445

Table 3. Friction velocity and Kármán number for each case studied.

Figure 5 shows the evolution of the mean axial component of the velocity profile in the radial direction for all the simulations carried out. Both u_x^+ and ξ^+ are expressed in wall-units. This result confirms that, for all the studied cases, the mean axial velocity profile scales with the friction velocity and collapse according to both the law-of-the-wall and the values of DNS data [13] and experimental data [4] . Unlike channel flow, several studies [3, 13] have shown that the pipe flow does not follow the logarithmic region close to the pipe centre. This behaviour is more important as the Reynolds number increases. Different values of the parameters that define the logarithmic region may be used. In this study, B = 5.2 and κ = 0.41 have been chosen as suggested by Nagib and Chauhan [38].

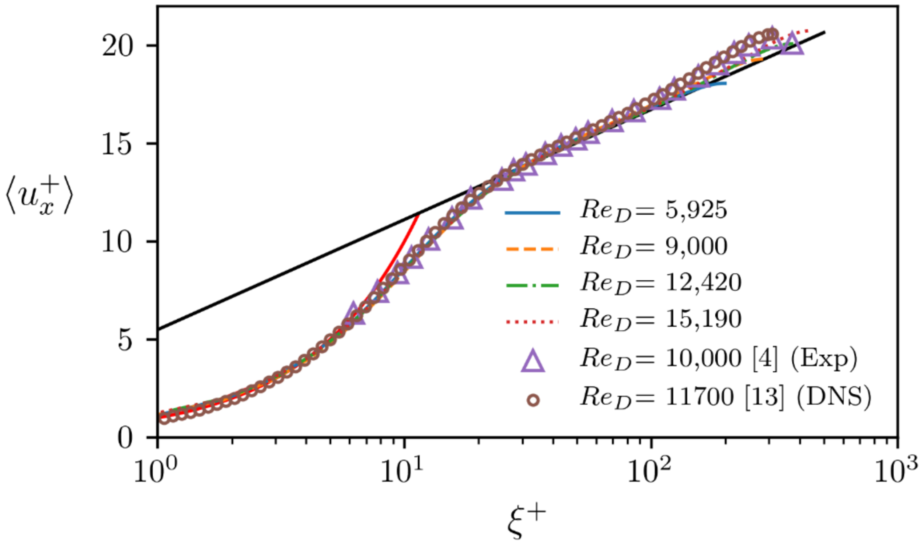

Figure 5: Mean axial velocity profile in wall units for each case studied.

Together with the velocity profiles, the standard deviation of the velocity field near the wall is important to characterize the turbulent intensity. Figure 6 depicts the axial component of the root mean squared velocity (x,rms+) for all the studied cases. Again, results are compared against DNS data from El Khoury et al. [13] and experimental data from den Toonder [4]. It is important to note that the maximum value of $u^+_{x,rms}$ for all the tested conditions is practically obtained at the same location (when expressed in wall-units) than the one obtained through DNS and experiments. It may also be noticed that the peak value of the $u^+_{x,rms}$ increases with the Reynolds number. This behaviour has been reported in different studies [13–15], but still remains an open question concerning this kind of flows. Nevertheless, the maximum values reached are slightly different at low Reynolds number, having a small underestimation of the peak of this parameter.

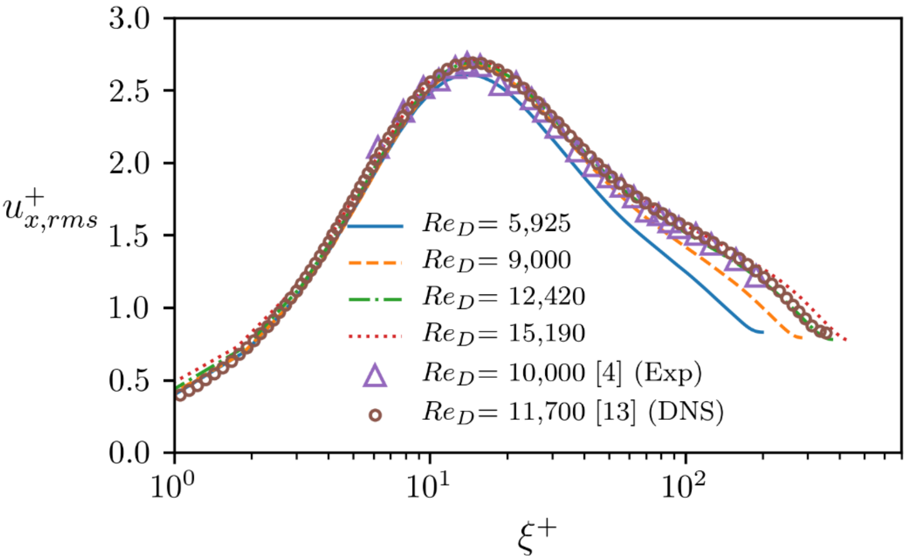

Figure 6: Root mean squared velocity in the streamwise direction for each case studied.

Finally, in order to assess the pressure drop inside the pipe, it is relevant to compare the friction factor evaluated from the friction velocity ($f = 8\,u_\tau^2/U_b^2$) with the Blasius or the Colebrook laws [39]. Figure 7 plots the friction factor values obtained from all numerical simulations against the Reynolds number. Their close resemblance to the values suggested by the Blasius and ColeBrook (particularized for a roughness factor equal to 0) laws implies that the turbulent behaviour near the wall is properly captured. It is interesting to point out that, when the Reynolds number increases, the values obtained match the Colebrook law more closely than the Blasius law.

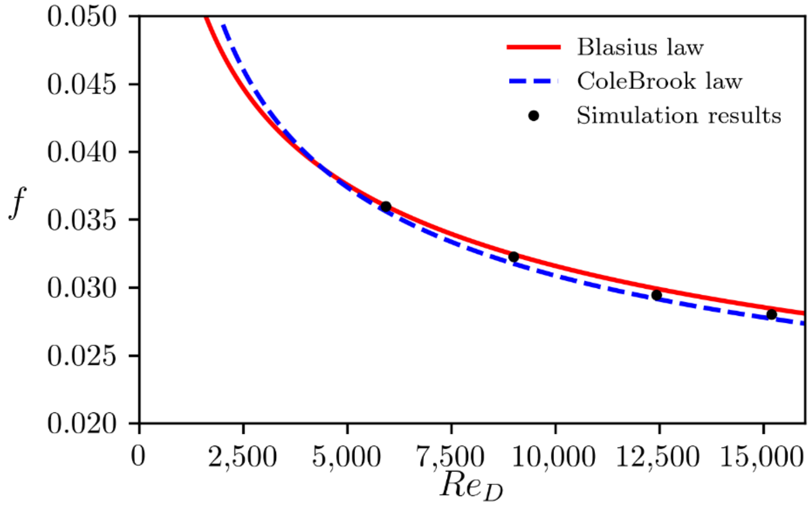

Figure 7: Friction Factor obtained from the simulations against the Blasius and Colebrook laws.

4.2. Detection and analysis of Vortex

By studying the contours of the λ_2 criterion, it is possible to study the distribution of vortex cores detected within the domain. It must be noted that the values of λ_2 usually fall within a wide range of numbers for this kind of studies. Hence, in order to compare and distinguish the distribution of the vortex structures for all the conditions tested, two different approaches have been performed. On the one hand, the same threshold value has been set for all the operating conditions. In this case, if the chosen threshold was too high, no vortex would appear at low Reynolds; if it was too low, the different vortex would start merging, obtaining a chaotic pattern not representative of the structure distribution. With this considerations, the threshold value for this approach is set to $\lambda_2 = -\,1e^{13}$ for all the studied cases. On the other hand, being that the values obtained from the λ_2 criterion increase with the Reynolds number, a relative threshold has been used to have a proportional vortex definition for all cases. An average of the minimum λ_2 is first performed for each case. Then, the 10% of this value is chosen as a threshold, this value is chosen to coincide for the $Re_D = 5{,}925$ condition so the chosen values are $-1e^{13}$, $-1.4e^{13}$, $-2.44e^{13}$ and $-3.1e^{13}$ when increasing the Reynolds number.

First, qualitative results are shown in order to demonstrate the influence of the Reynolds number on the generation of turbulent structures. Figure 8 represents the contours of λ_2 in a streamwise direction for all the tested conditions. It must be noticed that, as the Reynolds number increases, so does the number of structures. Nevertheless, their individual mean volume seems to decrease.

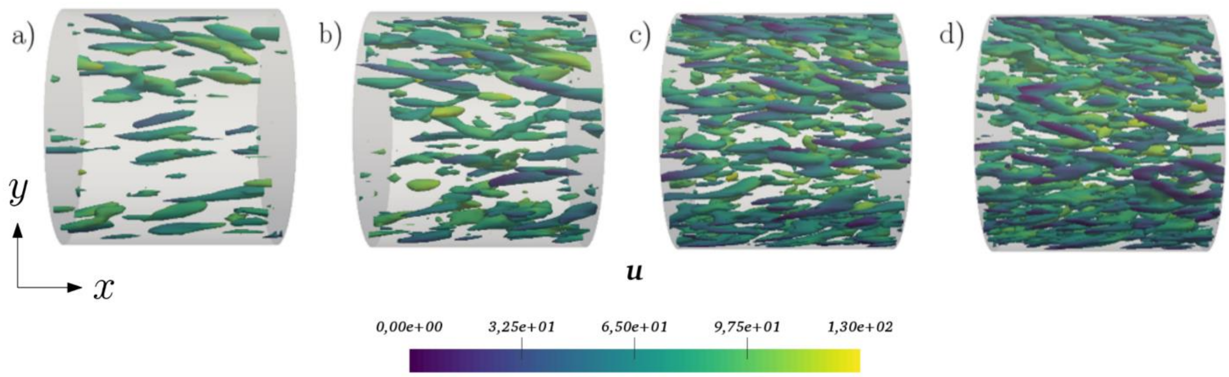

Figure 8: Iso-contours of $\lambda_2 = -1e^{13}$ in the XY plane for a) Re_D = 5,925, b) Re_D= 9,000, c) Re_D = 12,420, d) Re_D = 15,190 coloured by velocity in m/s.

In order to visualize the radial distribution, a perpendicular representation is shown in Figure 9. It is interesting to point out that the structures are mainly found near the wall and around the half of the pipe radius for all cases, leaving a void of turbulent structures at the pipe core. This result confirms the qualitative findings of Figure 8 in terms of number of structures and mean volume of the individual structures as a function of Re_D.

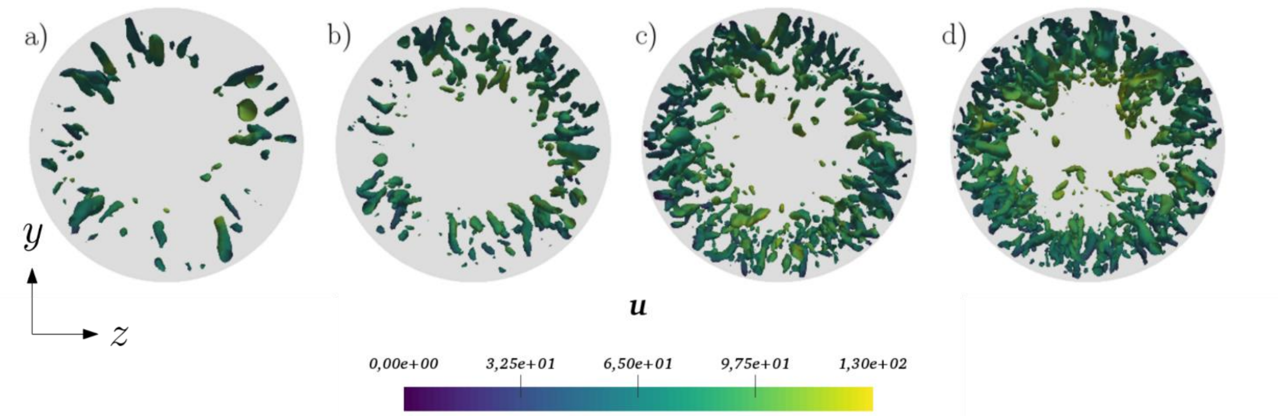

Figure 9: Iso-contours of $\lambda_2 = -1e^{13}$ in the YZ plane for a) Re_D = 5,925, b) Re_D = 9,000, c) Re_D = 12,420, d) Re_D = 15,190 coloured by velocity in m/s.

Once the qualitative results have been shown, a vortex detection algorithm is used to count these structures and sort them by volume and radial position. In order to get a reliable time average distribution, one snapshot per washout has been saved along 200 consecutive washouts. When computing the iso-surface extraction, some regions with a very small volume appear (as can be seen at Figure 9). Those small contours defined by only a few points have a numerical base. In order to clean the results from numerical noise, a minimum volume of two characteristic cells is set. Other than detecting the number of structures, Probability Density Functions (PDF) for both the total structures detected by volume and by radial position have also been obtained. These PDF discard the effect of the total amount of structures and allow directly comparing the vortex size and radial distribution. Figure 10 shows the results of applying this algorithm in terms of volume to all the cases studied for both λ_2 threshold criteria. Hence, upper figures from Figure 10 show the number of vortex structures (N_s) sorted by volume, whereas bottom figures depict the volume PDFs. Also, left figures correspond to the absolute threshold approach, whereas the right ones correspond to the relative threshold study. Starting with the volume distribution, the absolute threshold shows an increase of the total number of structures with the Reynolds number for the complete range of volumes, as hinted through the iso contours plotted in Figures 8 and 9. On the other hand, the relative threshold approach dilutes the bigger structures when increasing the Reynolds number. The reason behind these two different behaviours lies on the fact that the absolute threshold is lower than the relative one used, so that the bigger structures that appear at higher Reynolds correspond to less turbulent structures that are 'filtered' when increasing the value of this parameter. Nevertheless, bottom figures from Figure 10 show very similar PDF for the structures volume distribution, where the smallest scales increase its importance as the Reynolds number increases and the bigger ones are more present at lower Reynolds number. This also agrees with the findings from Figures 8 and 9 that each individual structure seemed to be qualitatively bigger at low Reynolds. Consequently, as the Reynolds number increases, the number of structures increases globally (i.e. for any volume size considered), but the probability of a given structure to be big quantitatively decreases.

Analogously, Figure 11 shows the same composition from Figure 10 but in terms of radial distribution (i.e. sorted by the radial position of the vortex centre). The radial distribution depicted in the upper plots from Figure 11 shows that the number of structures detected increases with the Reynolds number, regardless of the radial position considered when applying the absolute threshold. When applying the relative threshold, in turn, the number of structures detected near the wall is higher at high Reynolds number, but lower when moving towards the pipe centre. Bottom figures from Figure 11 display the probability of finding a structure at each radial position. In contrast with Figure 10, where both approaches led to similar PDFs, the obtained PDFs show different radial probability patterns depending on the λ_2 threshold criterion used. The absolute threshold approach shows a maximum location shift towards the wall as the Reynold number increases, and around $\xi = 0.3$ the higher Reynolds conditions show higher PDF values. This means that, even though the volume distribution is not highly affected by Re_D, the radial distribution is more spread the higher the Reynolds number. In contrast, when applying the relative threshold, the radial distribution tends to gather near the maximum peak and the dispersion towards the pipe centre disappears when increasing the Reynolds number. Even though this behaviour can seem contradictory at first sight, it can be understood when comparing both the volume and the radial distributions. The analysis from Figure 10 stated that the bigger structures at higher Reynolds number were less turbulent than the smaller ones because they were filtered when the λ_2 increased in the relative threshold approach. These filtered structures were the ones that spread towards the pipe centre in Figure 11, which is consistent with the fact that the very large structures are located near the centre [10] when the turbulence increases. This reasoning is in turn consistent with the vortex distributions qualitatively observed in Figure 9.

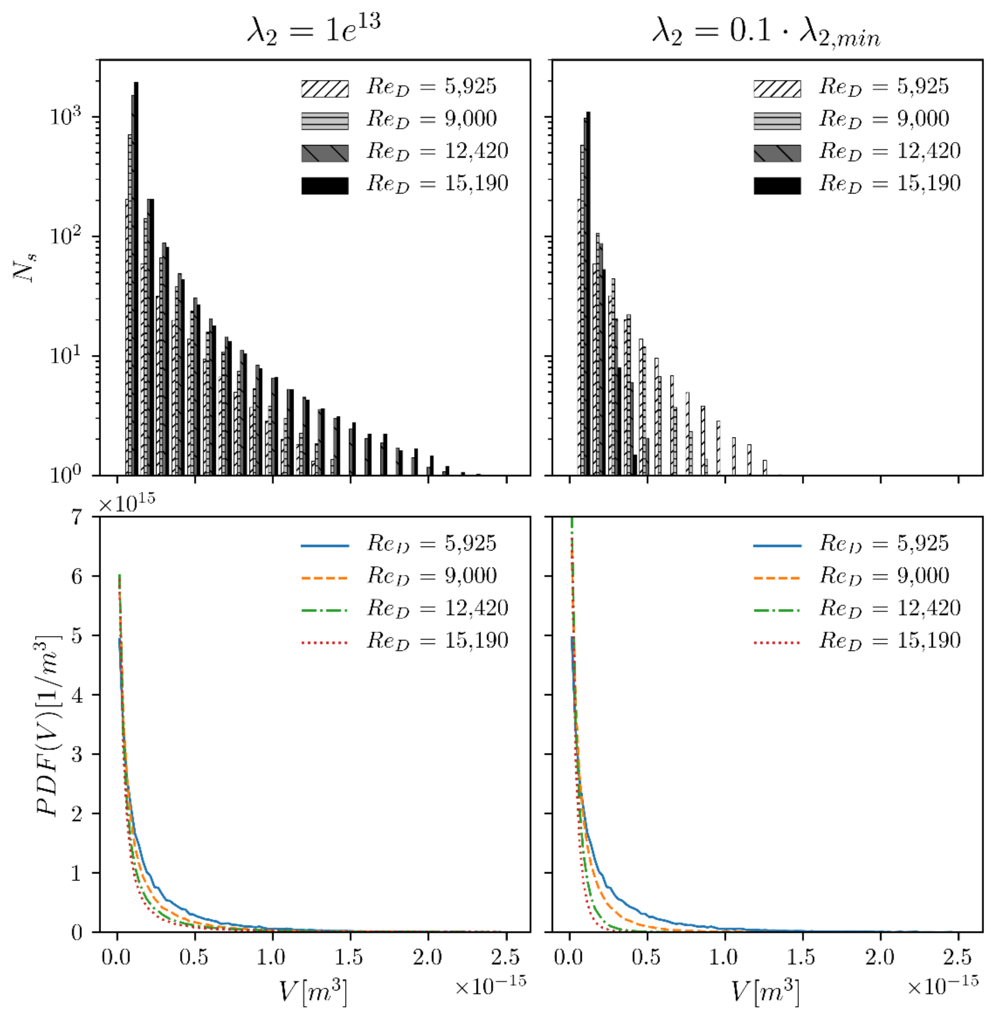

Figure 10: Left, absolute threshold approach; right, relative threshold approach. Upper: time averaged number of structures sorted by its volume for each case studied; bottom: volume PDF for each case studied.

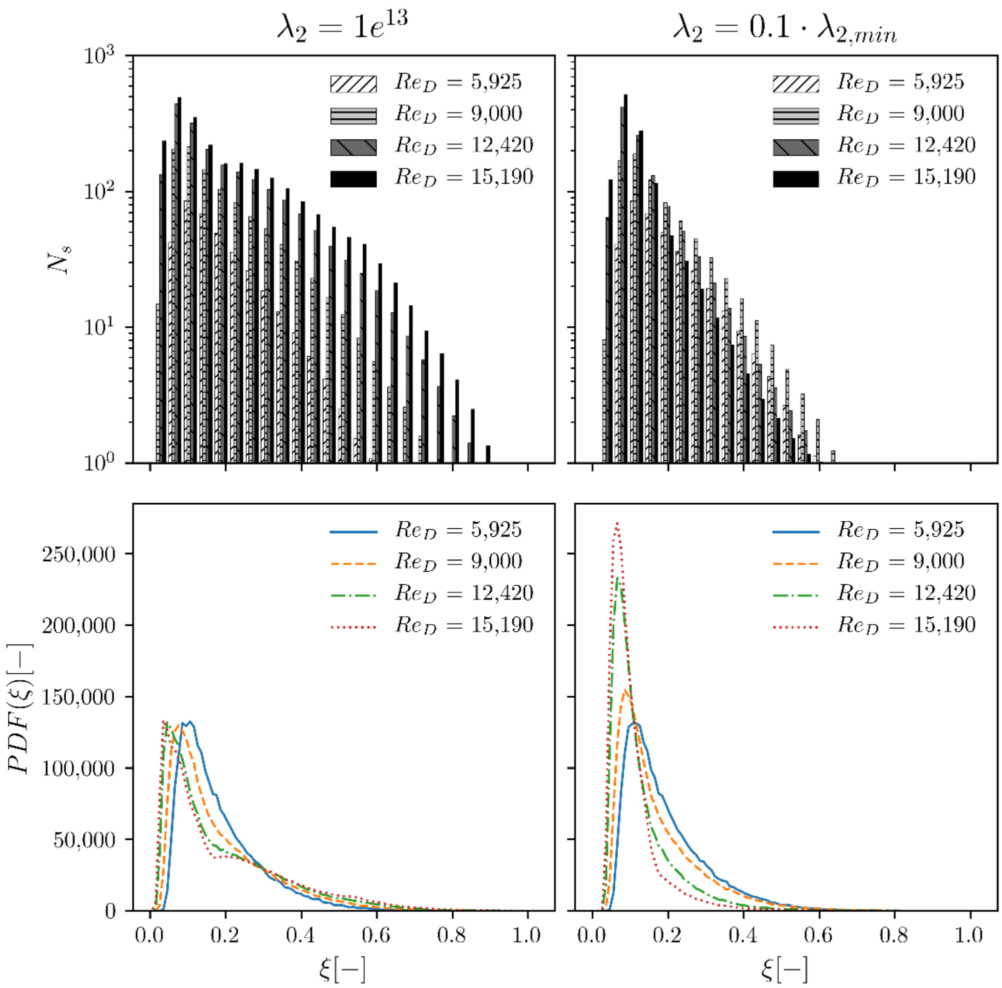

Figure 11: Left, absolute threshold approach; right, relative threshold approach. Upper: time averaged number of structures sorted by its radial for each case studied; bottom: radial position PDF for each case studied.

Finally, the same approach has been carried out using the Q-criterion to detect and sort the turbulent structures. A comparison among the λ_2 and Q-criterion has been made for the Re_D = 9,000 condition. Please note that $Q = 1e^{13}$ has been used as the threshold value to detect the contours (same absolute value than the one used for the λ_2 criterion). The comparison has been done in terms of PDF of volume and radial distribution, as depicted in Figure 12. Figure 12a) presents the PDF of the number of structures detected for different volumes, where it can be clearly seen that the trends obtained through both criteria collapse perfectly. On the other hand, Figure 12b) shows that the peak shape is slightly sharper with the Q-criterion, although its radial position remains at the same distance from the wall and the main shape is quite similar.

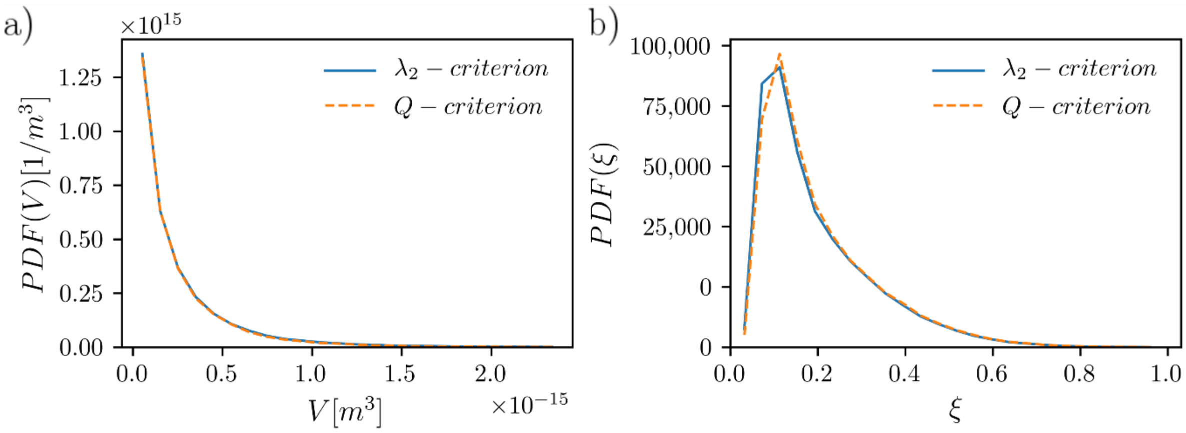

Figure 12: a) Volume PDF for Re_D = 9,000 for both vortex detecting methods, b) Radial PDF for Re_D = 9,000 for both vortex detecting methods.

5. CONCLUSIONS

LES of fully developed turbulent pipe flow have been performed at low Reynolds number, from Re_D = 5,925 to 15,190 based on the pipe diameter. The Navier-Stokes equations are solved with the pisoFoam solver (OpenFOAM code) using the WALE SGS model. The assessment of the computational LES calculations has been done by evaluating the IQ_k quality index, reporting values above 0.8 in all the radial positions for all the simulated cases.

Computing the mean statistics for the different cases showed that the steady state was achieved for all the simulations carried out. The turbulent processes are found to be well captured, despite small discrepancies in the streamwise inner peak of the root mean squared velocity. As the Reynolds number increases, so do the turbulence and the inner $u^+_{x,rms}$, as stated in the literature [8-10].

When it comes to the vortex structures, two different approaches based on the λ_2 criterion have been used to get the volume and radial distribution of the vortex within the flow. On the one hand, the same threshold has been used to define the vortex core at all operating conditions; on the other hand, a relative threshold depending on the minimum value of λ_2 for each tested case has been used. Regarding the number of detected structures, both methods detect an increase in the number of structures generated then the turbulence increases. Nevertheless, the absolute threshold procedure exhibits an increase of the maximum volume detected with the Reynolds Number, whereas the relative threshold procedure shows that the lower Reynolds conditions generate the bigger structures. This means that the lower value of the threshold at high Reynolds conditions is linked to bigger structures that are less turbulent. This theory is confirmed when looking at the radial distribution of the vortex structures. Using an absolute threshold, the detected structures spread towards the pipe centre when increasing the Reynolds number, behaviour that is not showed when using a relative threshold value. This means that the bigger structures, which are less turbulent, are located away from the wall. Finally, the peak values at which the structures collapse are maintained using both approaches, their location shifting towards the wall as the Reynolds number increases. In addition, results obtained using λ_2 criterion with the absolute threshold approach and the ones obtained using the Q criterion (computed for a single operating condition) are quite similar presenting the same volume PDF and virtually the same radial distribution.

These results can be used to compare the structures generated by a pipe flow synthetic boundary condition when using them or when generating new synthetic turbulence models for these cases.

Lastly, the results presented on this paper expect to be an accessible way of comparing and validating the structures generated by a pipe flow when using a synthetic boundary condition or when developing new synthetic turbulence models. As reported in the literature [26, 40], these structures play a significant role on spray atomization processes. These works stated that an increase in the amount of these vortex cores and their proximity to the gas-liquid interface cause an increase in the spray core instabilities, finally leading to a better atomization. The findings of the present investigation thus open a new insight on further atomization studies, also being relevant for other applications.

COMPLIANCE WITH ETHICAL STANDARDS

Funding: This research has been funded by the Spanish Ministerio de Ciencia e Innovación through the projects RTI2018-099706-B-100: "Estudio de la atomización primaria mediante simulaciones DNS y técnicas ópticas de muy alta resolución" and EQC2018-004605-P: "Estudio del proceso de inyección en atmosferas presurizadas". González-Montero L.A. is partially supported though the contract FPI – Subprograma 2 of the Universitat Politècnica de València.

Competing interests: the authors declare that they have no conflict of interest.

REFERENCES

1. Townsend AA (1980) The structure of turbulent shear flow, 2nd ed. Cambridge University Press, Cambridge
2. Marusic I, McKeon BJ, Monkewitz PA, Nagib HM, Smits AJ, Sreenivasan KR (2010) Wall-bounded turbulent flows at high Reynolds numbers: Recent advances and key issues. Phys Fluids 22:1–24 . https://doi.org/10.1063/1.3453711
3. Eggels JGM, Unger F, Weiss MH, Westerweel J, Adrian RJ, Friedrich R, Nieuwstadt FTM (2006) Fully developed turbulent pipe flow: a comparison between direct numerical simulation and experiment. J Fluid Mech 268:175–210 . https://doi.org/10.1017/S002211209400131X
4. den Toonder JMJ, Nieuwstadt FTM (1997) Reynolds number effects in a turbulent pipe flow for low to

moderate Re. Phys Fluids 9:3398–3409 . https://doi.org/10.1063/1.869451

5. Zagarola M V., Smits AJ (1997) Scaling of the Mean Velocity Profile for Turbulent Pipe Flow. Phys Rev Lett 78:239–242 . https://doi.org/10.1103/PhysRevLett.78.239

6. Hultmark M, Vallikivi M, Bailey SCC, Smits AJ (2012) Turbulent pipe flow at extreme reynolds numbers. Phys Rev Lett 108:1–5 . https://doi.org/10.1103/PhysRevLett.108.094501

7. Talamelli A, Persiani F, H M Fransson J, Alfredsson PH, V Johansson A, M Nagib H, Rüedi J-D, R Sreenivasan K, A Monkewitz P (2009) CICLoPE—a response to the need for high Reynolds number experiments. Fluid Dyn Res 41:021407 . https://doi.org/10.1088/0169-5983/41/2/021407

8. Örlü R, Fiorini T, Segalini A, Bellani G, Talamelli A, Alfredsson PH (2017) Reynolds stress scaling in pipe flow turbulence - First results from CICLoPE. Philos Trans R Soc A Math Phys Eng Sci 375: . https://doi.org/10.1098/rsta.2016.0187

9. Kim J, Moin P, Moser R (1987) Turbulence statistics in fully developed channel flow at low Reynolds number. J Fluid Mech 177:133–166 . https://doi.org/10.1017/S0022112087000892

10. Kim KC, Adrian RJ (1999) Very large-scale motion in the outer layer. Phys Fluids 11:417–422 . https://doi.org/10.1063/1.869889

11. Wu X, Moin P (2008) A direct numerical simulation study on the mean velocity characteristics in turbulent pipe flow

12. Wu X, Baltzer JR, Adrian RJ (2012) Direct numerical simulation of a 30R long turbulent pipe flow at R + = 685: Large-and very large-scale motions. J Fluid Mech 698:235–281 . https://doi.org/10.1017/jfm.2012.81

13. El Khoury GK, Schlatter P, Noorani A, Fischer PF, Brethouwer G, Johansson A V. (2013) Direct numerical simulation of turbulent pipe flow at moderately high reynolds numbers. Flow, Turbul Combust 91:475–495 . https://doi.org/10.1007/s10494-013-9482-8

14. Chin C, Ooi ASH, Marusic I, Blackburn HM (2010) The influence of pipe length on turbulence statistics computed from direct numerical simulation data. Phys Fluids 22:115107 . https://doi.org/10.1063/1.3489528

15. Klewicki J, Chin C, Blackburn HM, Ooi A, Marusic I (2012) Emergence of the four layer dynamical regime in turbulent pipe flow. Phys Fluids 24:045107 . https://doi.org/10.1063/1.3702897

16. Schlatter P, Örlü R (2012) Turbulent boundary layers at moderate Reynolds numbers: inflow length and tripping effects. J Fluid Mech 710:5–34 . https://doi.org/10.1017/jfm.2012.324

17. Jiménez J, Hoyas S (2008) Turbulent fluctuations above the buffer layer of wall-bounded flows. J Fluid Mech

611:215–236 . https://doi.org/10.1017/S0022112008002747

18. Kim J (2012) Progress in pipe and channel flow turbulence, 1961–2011. J Turbul 13:N45 . https://doi.org/10.1080/14685248.2012.726358

19. Hellström LHO, Marusic I, Smits AJ (2016) Self-similarity of the large-scale motions in turbulent pipe flow. J Fluid Mech 792:R1 . https://doi.org/10.1017/jfm.2016.100

20. Abreu LI, Cavalieri AVG, Schlatter P, Vinuesa R, Henningson DS (2020) Spectral proper orthogonal decomposition and resolvent analysis of near-wall coherent structures in turbulent pipe flows. J Fluid Mech. https://doi.org/10.1017/jfm.2020.445

21. Hwang J, Sung HJ (2019) Wall-attached clusters for the logarithmic velocity law in turbulent pipe flow. Phys Fluids 31: . https://doi.org/10.1063/1.5096433

22. Dhamankar NS, Blaisdell GA, Lyrintzis AS (2018) Overview of turbulent inflow boundary conditions for large-eddy simulations. AIAA J 56:1317–1334 . https://doi.org/10.2514/1.J055528

23. Klein M, Sadiki A, Janicka J (2003) A digital filter based generation of inflow data for spatially developing direct numerical or large eddy simulations. J Comput Phys 186:652–665 . https://doi.org/10.1016/S0021-9991(03)00090-1

24. Ménard T, Tanguy S, Berlemont A (2007) Coupling level set/VOF/ghost fluid methods: Validation and application to 3D simulation of the primary break-up of a liquid jet. Int J Multiph Flow 33:510–524 . https://doi.org/10.1016/j.ijmultiphaseflow.2006.11.001

25. Bini M, Jones WP (2008) Large-eddy simulation of particle-laden turbulent flows. J Fluid Mech 614:207–252 . https://doi.org/10.1017/S0022112008003443

26. Payri R, Salvador FJ, Gimeno J, Crialesi-Esposito M (2019) Comparison of mapped and synthetic inflow boundary conditions in Direct Numerical Simulation of sprays. In: ILASS - Europe 2019, 29th Conference on Liquid Atomization and Spray Systems. Paris, France

27. Warncke K, Gepperth S, Sauer B, Sadiki A, Janicka J, Koch R, Bauer HJ (2017) Experimental and numerical investigation of the primary breakup of an airblasted liquid sheet. Int J Multiph Flow 91:208–224 . https://doi.org/10.1016/j.ijmultiphaseflow.2016.12.010

28. ECN (2010) Engine Combustion Network. In: https://ecn.sandia.gov/diesel-spray-combustion/. www.sandia.gov/ecn/

29. Nicoud F, Ducros F (1999) Subgrid-Scale Stress Modelling Based on the Square of the Velocity Gradient

Tensor. Flow, Turbul Combust 62:183–200 . https://doi.org/10.1023/A:1009995426001
30. Issa R. I (1986) Solution of the implicitly discretised fluid flow equations by operator-splitting. J Comput Phys 62:40–65 . https://doi.org/10.1016/0021-9991(86)90099-9
31. (2015) OpenFOAM v3.0.0
32. Jeong J, Hussain F, Jinhee J, Fazle H (1995) On the identification of a vortex. J Fluid Mech 285:69–94 . https://doi.org/doi:10.1017/S0022112095000462
33. Hunt JCR, Wray a a, Moin P (1988) Eddies, streams, and convergence zones in turbulent flows. In: Center for Turbulence Research, Proceedings of the Summer Program. San Francisco, USA, pp 193–208
34. Pope S (2009) Turbulent Flows, sixth. Cambridge University Press
35. Sagaut P (2006) Large eddy simulation for incompressible flows: an introduction. Springer Science & Business Media
36. Celik I, Klein M, Janicka J (2009) Assessment measures for engineering LES applications. J Fluids Eng Trans ASME 131:0311021–03110210 . https://doi.org/10.1115/1.3059703
37. Wagner C, Hüttl T., Friedrich R (2001) Low-Reynolds-number effects derived from direct numerical simulations of turbulent pipe flow. Comput Fluids 30:581–590 . https://doi.org/10.1016/S0045-7930(01)00007-X
38. Nagib HM, Chauhan KA (2008) Variations of von Kármán coefficient in canonical flows. Phys Fluids 20:101518 . https://doi.org/10.1063/1.3006423
39. Moody L, Princeton N (1944) Friction Factors for Pipe Flow. Trans ASME 66:671–684
40. Hasslberger J, Ketterl S, Klein M, Chakraborty N (2019) Flow topologies in primary atomization of liquid jets: A direct numerical simulation analysis. J Fluid Mech 859:819–838 . https://doi.org/10.1017/jfm.2018.845